
Alkenone isotopes show evidence of active carbon concentrating mechanisms in coccolithophores as aqueous carbon dioxide concentrations fall below $7 \mu\text{molL}^{-1}$

Marcus P.S. Badger

School of Environment, Earth & Ecosystem Sciences, The Open University, Milton Keynes, MK7 6AA, UK
marcus.badger@open.ac.uk

This version of the manuscript was submitted to *Biogeosciences* and published as a discussion paper in *Biogeosciences Discussions* for open peer review. The interactive discussion and version of record can be found at <https://doi.org/10.31223/osf.io/3ywqd> and a revised paper will be uploaded here following peer review.

Alkenone isotopes show evidence of active carbon concentrating mechanisms in coccolithophores as aqueous carbon dioxide concentrations fall below $7 \mu\text{molL}^{-1}$

Marcus P. S. Badger¹

¹School of Environment, Earth & Ecosystem Sciences, The Open University, Milton Keynes, MK7 6AA, UK

Correspondence: Marcus P. S. Badger (marcus.badger@open.ac.uk)

5 **Abstract.**

Coccolithophores and other haptophyte algae acquire the carbon required for metabolic processes from the water in which they live. Whether carbon is actively moved across the cell membrane via a carbon concentrating mechanism, or passively through diffusion, is important for haptophyte biochemistry. The possible utilisation of carbon concentrating mechanisms also has the potential to over-print one proxy method by which ancient atmospheric CO_2 is reconstructed using alkenone isotopes. Here I show that carbon concentrating mechanisms are likely used when aqueous carbon dioxide concentrations are below $7 \mu\text{molL}^{-1}$. I use published alkenone based CO_2 reconstructions from multiple sites over the Pleistocene, which allows comparison to be made with ice core CO_2 records. Interrogating these records reveal that the relationship between proxy- and ice core- CO_2 breaks down when local aqueous CO_2 concentration falls below $7 \mu\text{molL}^{-1}$. The recognition of this threshold explains why many alkenone based CO_2 records fail to accurately replicate ice core CO_2 records, and suggests the alkenone proxy is likely robust for much of the Cenozoic when this threshold was unlikely to be reached in much of the global ocean.

Copyright statement. This work is distributed under the Creative Commons Attribution 4.0 License.

1 **Introduction**

Alkenones are long-chain (C_{37-39}) ethyl- and methy- ketones (Figure 1; Brassell et al. (1986); Rechka and Maxwell (1987)) produced by a restricted group of photosynthetic haptophyte algae (Conte et al., 1994). Produced by a narrow group of organisms which live exclusively in the photic zone, alkenones allow probing of algal biogeochemistry, and as alkenones are often preserved in the sedimentary record, alkenones can also provide information about past environmental conditions. Two main proxy systems based on alkenone geochemistry exist, (1) for sea surface temperature (SST) relies on the changing degree of unsaturation of the C_{37} alkenone ($U_{37}^{K'}$) (Brassell et al., 1986) and (2) for atmospheric CO_2 , based on reconstructing the isotopic fractionation which takes place during photosynthesis (ϵ_p) using the carbon isotopic composition of the preserved alkenones (referred to throughout as $\text{CO}_{2(\epsilon_p-\text{alk})}$) (Laws et al., 1995; Bidigare et al., 1997).

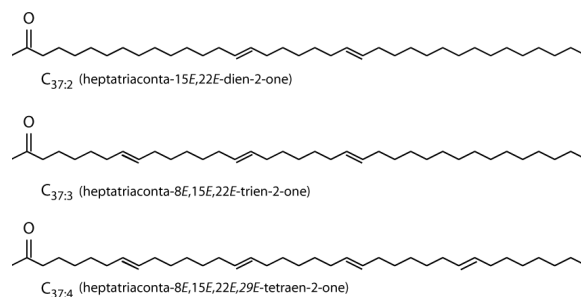


Figure 1. Alkenones are C_{37} unsaturated methyl ketones (Brassell et al., 1986; Reehka and Maxwell, 1987).

In the modern ocean alkenones are produced primarily by two dominant coccolithophore species; *Emiliania huxleyi* and *Gephyrocapsa oceanica*. *E. huxleyi* first appeared 290 kyr ago, and began to dominate over *G. oceanica* around 82 kyrs ago (Gradstein et al., 2012; Raffi et al., 2006). However alkenones are commonly found in sediments throughout the Cenozoic, with the oldest reported detections from mid-Albian aged black shales (Farrimond et al., 1986). Prior to the evolution of *G. oceanica* alkenones were most likely produced by other closely related species from the Noelarhabdaceae family (Marlowe et al., 1990; Volkman, 2000).

Proxies for atmospheric CO_2 including $CO_{2(\epsilon_p-alk)}$, those based on the $\delta^{11}B$ of planktic foraminifera, geochemical modelling and stomatal density, broadly agree that over the Cenozoic atmospheric pCO_2 declined from high levels ($>1000 \mu atm$) in the "greenhouse" worlds of the Paleocene and Eocene to close to modern day values (around $400 \mu atm$) in the Pliocene (Pagani et al., 2005, 2011; Pearson et al., 2009; Anagnostou et al., 2016; Foster et al., 2017; Sosdian et al., 2018; Super et al., 2018; Zhang et al., 2013; Beerling and Royer, 2011). However recently discrepancies have emerged between the alkenone and other CO_2 proxies at the moderate to low levels of atmospheric CO_2 of the Pleistocene (i.e. $<400 \mu atm$; Badger et al. (2019, 2013a) and compare Badger et al. (2013b) and Pagani et al. (2009) with Martínez-Botí et al. (2015)). Whilst the longstanding difference between alkenone (Pagani et al., 1999), $\delta^{11}B$ (Foster et al., 2012) and stomatal proxies (Kürschner et al., 2008) in the Miocene CO_2 reconstructions appears to be resolved with new SST records (Super et al., 2018), differences remain in the Pliocene (Pagani et al., 2009; Badger et al., 2013b; Martínez-Botí et al., 2015) and Pleistocene (Badger et al., 2019).

One plausible reason for these discrepancies is the action of active carbon concentrating mechanisms (CCMs) in the haptophytes. These are potentially important as $CO_{2(\epsilon_p-alk)}$ assumes purely passive uptake of carbon into the haptophyte cell (Laws et al., 1995; Bidigare et al., 1997). The potential for CCMs to be active and to effect $CO_{2(\epsilon_p-alk)}$ has long been known (Laws et al., 1997, 2002; Cassar et al., 2006) and recent work has refocussed efforts on understanding CCMs in $CO_{2(\epsilon_p-alk)}$ (Bolton et al., 2012; Bolton and Stoll, 2013; Stoll et al., 2019; Zhang et al., 2019, 2020). In this study I use the now large number of published $CO_{2(\epsilon_p-alk)}$ records which overlap with ice core records of atmospheric CO_2 (Tables 1 & 2) to explore the relationship between $CO_{2(\epsilon_p-alk)}$ and CCMs in the Pleistocene, where our understanding of atmospheric CO_2 is best.

Table 1. Sites with Pleistocene $\text{CO}_2(\epsilon_p\text{-alk})$ records. Note that the MANOP Site C record was generated to track changes in surface water-atmosphere equilibrium not atmospheric $p\text{CO}_2$, so although included here for completeness, is not included in the analysis

Site	Latitude	Longitude	Reference
ODP 999	12° 44.639' N	78° 44.360' W	Badger et al. (2019)
ODP 925	4° 12.249' N	43° 29.334' W	Zhang et al. (2013)
DSDP 619	27° 11.61' N	91° 24.54' W	Jasper and Hayes (1990)
MANOP Site C	0° 57.2" N	138° 57.3' W	Jasper et al. (1994)
NIOB 464	22° 15.4' N	63° 31.1'E	Palmer et al. (2010)
GeoB 1016-3	11° 46' S	11° 40' E	Andersen et al. (1999)
05PC-21	37° 30.11'N	129° 42.86'E	Bae et al. (2015)

Table 2. Sources of ice core data, as compiled by Bereiter et al. (2015). WAIS - West Antarctic Ice Sheet, TALDICE - TALos Dome Ice CorE, EDML - EPICA Dronning Maud Land

Age interval (kyr)	Ice core location	Reference
-0.051-1.8	Law Dome	Rubino et al. (2013)
1.8-2	Law Dome	MacFarling Meure et al. (2006)
2-11	Dome C	Monnin et al. (2001, 2004)
11-22	WAIS	Marcott et al. (2014)
22-40	Siple Dome	Ahn and Brook (2014)
40-60	TALDICE	Bereiter et al. (2012)
60-115	EDML	Bereiter et al. (2012)
105-155	Dome C Sublimation	Schneider et al. (2013)
155-393	Vostok	Petit et al. (1999)

2 Materials and Methods

50 2.1 Calculating CO_2 from alkenone $\delta^{13}\text{C}$: The $\text{CO}_2(\epsilon_p\text{-alk})$ proxy

Multiple records of $\text{CO}_2(\epsilon_p\text{-alk})$ have been published for the Pleistocene (Figure 2, Table 1) allowing direct comparison with ice core based CO_2 records (Table 2). These records are globally distributed in longitude, but are concentrated at low latitude sites, largely as there is a general preference for sites which have (in the modern ocean) surface waters close to equilibrium with the atmosphere (Figure 2, Table 1). In longer term palaeoclimate studies there has also been a preference for low latitude, gyre sites in the belief that these sites are more likely to be oceanographically stable over long time intervals (Pagani et al., 1999). Most of the records included here (Table 1, Figure 2) were generated with the aim to reconstruct atmospheric CO_2 , however one, the MANOP C Site of Jasper et al. (1994), was used to explicitly reconstruct changing disequilibrium due to oceanographic frontal changes over time, and so is excluded from the following analysis.

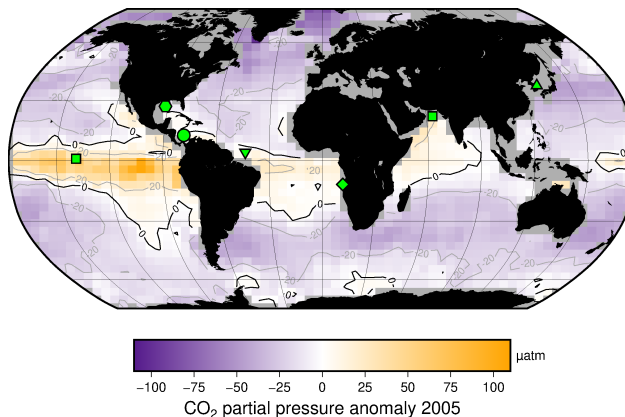


Figure 2. Study sites relative to mean annual surface ocean CO₂ disequilibrium for 2005. Sites are globally distributed in longitude but restricted in latitude, as generally sites are chosen to be close to surface water equilibrium with the atmosphere. Sites used for this study are indicated, over the mean annual surface ocean disequilibrium for 2005 calculated from Takahashi et al. (2014). The MANOP C Site (Jasper et al., 1994) was chosen to study the disequilibrium at that site, so is shown here but not used in the following analyses. Site symbols are used throughout the figures: ODP 999 - circle, 05PC-21 - triangle, ODP 925 - inverted triangle, DSDP 619 - hexagon, MANOP Site C - square, NIOP 464 - star, GeoB 1016-3 - diamond.

Whilst these sites do only span a relatively small latitudinal extent, the diversity of settings does allow for investigation of any secondary controls on alkenone $\delta^{13}\text{C}$ ($\delta^{13}\text{C}_{\text{alkenone}}$). In particular, differences in oceanographic setting and SST to test the hypothesis that low $[\text{CO}_2]_{(\text{aq})}$ breaks the relationship between $\delta^{13}\text{C}_{\text{alkenone}}$ and atmospheric CO₂, as might be expected if haptophytes are able to actively uptake carbon from seawater to meet metabolic demand – i.e. activate CCMs.

To facilitate fair comparison between sites and consistent comparison with the ice core records, all CO₂(ϵ_p -alk) records I recalculated using a consistent approach. The approach is based on Bidigare et al. (1997) which updated the initial approach of Jasper and Hayes (1990) to CO₂(ϵ_p -alk).

This approach removes some additional corrections used in the original publication of the records (such as growth rate adjustment for NIOP 464 (Palmer et al., 2010)) but does allow for direct comparison to be made.

An overview of how CO₂(ϵ_p -alk) data are typically generated is given in Badger et al. (2013b).

Briefly, to calculate ϵ_p requires the carbon isotopic composition of the dissolved CO₂ ($\delta^{13}\text{C}_{\text{CO}_2(\text{aq})}$) and haptophyte biomass ($\delta^{13}\text{C}_{\text{org}}$). The isotopic fractionation between $\delta^{13}\text{C}_{\text{alkenone}}$ and $\delta^{13}\text{C}_{\text{org}}$ is first corrected assuming a constant fractionation ($\epsilon_{\text{alkenone}}$) of 4.2 ‰ (Popp et al., 1998; Bidigare et al., 1997):

$$\epsilon_{\text{alkenone}} = \frac{\delta^{13}\text{C}_{\text{alkenone}} + 1000}{\delta^{13}\text{C}_{\text{org}} + 1000} - 1 \quad (1)$$

The isotopic composition of dissolved inorganic carbon (DIC) is estimated using (ideally) the $\delta^{13}\text{C}$ of planktic foraminifera and the temperature-dependant fractionation between calcite and $[\text{CO}_2]_{(g)}$ experimentally determined by Romanek et al. (1992), where T is sea surface temperature in degrees Celsius (SST):

$$\varepsilon_{\text{calcite}-\text{CO}_2(g)} = 11.98 - 0.12T \quad (2)$$

The value the carbon isotopic composition of $\text{CO}_2(g)$ ($\delta^{13}\text{C}_{\text{CO}_2(g)}$) can then be calculated:

$$\delta^{13}\text{C}_{\text{CO}_2(g)} = \frac{\delta^{13}\text{C}_{\text{carbonate}} + 1000}{\varepsilon_{\text{calcite}-\text{CO}_2(g)}/1000 + 1} - 1000 \quad (3)$$

From this $\delta^{13}\text{C}_{\text{CO}_2(aq)}$ can be calculated using the relationship experimentally determined by Mook et al. (1974):

$$\varepsilon_{\text{CO}_2(aq)-\text{CO}_2(g)} = \frac{-373}{T + 273.15} + 0.19 \quad (4)$$

and

$$\delta^{13}\text{C}_{\text{CO}_2(aq)} = \left(\frac{\varepsilon_{\text{CO}_2(aq)-\text{CO}_2(g)}}{1000} + 1 \right) \cdot (\delta^{13}\text{C}_{\text{CO}_2(g)} + 1000) - 1000 \quad (5)$$

Finally ε_p can be calculated:

$$\varepsilon_p = \left(\frac{\delta^{13}\text{C}_{\text{CO}_2(aq)} + 1000}{\delta^{13}\text{C}_{\text{org}} + 1000} - 1 \right) \cdot 1000 \quad (6)$$

and from that $[\text{CO}_2]_{(aq)}$ is calculated using the isotopic fractionation during carbon fixation (ε_f) and 'b', which represents the summation of physiological factors:

$$[\text{CO}_2]_{(aq)} = \frac{b}{\varepsilon_f - \varepsilon_p} \quad (7)$$

Here ε_f is assumed to be a constant 25 ‰ (Bidigare et al., 1997). In the modern ocean the 'b' term, which accounts for physiological factors such as cell size and growth rate, shows a close correlation with $[\text{PO}_4^{3-}]$ (Bidigare et al., 1997; Pagani et al., 2009). However, the relationship between b, growth rate and $[\text{PO}_4^{3-}]$ has recently been questioned (Zhang et al., 2019, 2020) but for the purposes of this analysis is assumed to hold. This is discussed further below. Values for SST, $\delta^{13}\text{C}_{\text{alkenone}}$, $\delta^{13}\text{C}_{\text{carbonate}}$, salinity and $[\text{PO}_4^{3-}]$ are either taken from the original publications or estimated from modern ocean estimates (Takahashi et al., 2009; Antonov et al., 2010; Garcia et al., 2013; Locarnini et al., 2013).

Providing that the atmosphere is in equilibrium with surface water, the concentration of atmospheric CO₂ can be calculated
95 from [CO₂]_(aq), (and vice versa if atmospheric CO₂ is known) using Henry's law:

$$pCO_2 = \frac{[CO_2]_{(aq)}}{K_H} \quad (8)$$

The solubility coefficient (K_H) is dependant on salinity and SST, and here is calculated following the paramterization of Weiss (1970, 1974).

3 Results

100 3.1 Multi-site comparisons between CO₂(ε_p-alk) and the ice core records

Across the six sites included in this analysis, there are 217 CO₂(ε_p-alk)-based estimates of atmospheric CO₂ over the past 260 Ka for comparison with the ice core records (Table 2; Bereiter et al. (2015)). When all CO₂(ε_p-alk) estimates are considered together over 260 Ka, this compilation of proxy-based records fails to replicate the ice core record (Figure 3). This has already been noted at specific sites (e.g. Site 999 in the Caribbean Badger et al. (2019)) but this is the first time that all available records
105 coincident with the Pleistocene ice core records have been compiled using a common methodology. Notably the CO₂(ε_p-alk) based estimates are rarely lower than time-equivalent ice core estimate, but frequently higher. Given that haptophytes require carbon to satisfy metabolic demand, this is perhaps unsurprising; if at times of low carbon availibility haptophytes can switch from passive to active uptake to satisfy metabolic demand, it would be times of low atmospheric CO₂ (and so lower [CO₂(aq)]) when the active uptake is most likely to be needed. As CO₂(ε_p-alk)-based estimates of atmospheric CO₂ rely on the assumption
110 of a purely difusive uptake of carbon, it is therefore likely that the proxy would perform least well at times of low atmospheric CO₂.

The haptophyes do not directly interact with the atmosphere, obtaining their carbon from dissolved carbon. As it is not only atmospheric CO₂ which controls the concentration of dissolved carbon ([CO₂]_(aq)), but also temperature, alkalinity and other oceanographic factors which control the equilibrium state between surface waters at the atmosphere, (Figure 2) the multiple
115 sites in different settings now give the opportunity to test whether other factors are important in controlling the accuracy of CO₂(ε_p-alk).

To produce time-equivalent estimates of atmospheric CO₂ for comparison with the ice core records, a simple linear interpolation of the Bereiter et al. (2015) compilation was initially used (Figure 4). This assumes that both the age model of the ice core and the published age models of the sites are correct and equivalent. This is almost certainly not the case, and so for the
120 calculations below, a ±3000 year uncertainty is included for ages of both the ice core and CO₂(ε_p-alk) values. Figure 4 shows that CO₂(ε_p-alk)-based atmospheric CO₂ agree with ice core CO₂ at some sites and at some times, but not throughtout. Sites such as 05-PC21 (Bae et al., 2015) and DSDP Site 619 (Jasper and Hayes, 1990) perform quite well, throughtout, whilst others only appear to agree at higher values of CO₂, such as ODP Site 999 (Badger et al., 2019) and NIOP 464 (Palmer et al., 2010),

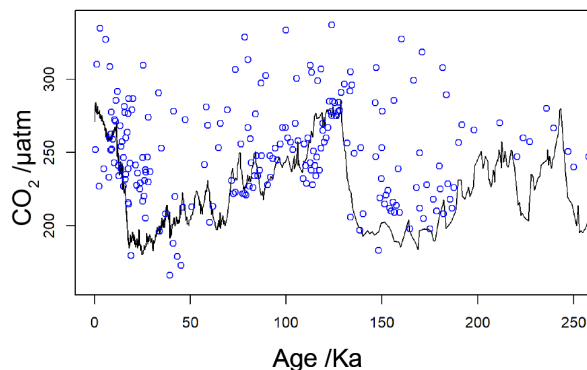


Figure 3. Compiled $\text{CO}_2(\varepsilon_p\text{-alk})$ -based estimates of atmospheric CO_2 over the past 260 Ka (blue circles), with the ice core compilation of Bereiter et al. (2015) shown as the solid black line. Full sources for the ice core and $\text{CO}_2(\varepsilon_p\text{-alk})$ records are in Tables 2 and 1

whilst at some locations there is very little overlap between the two methods of reconstructing CO_2 (such as ODP Site 925
125 (Zhang et al., 2013) and GElB 1016-3 (Andersen et al., 1999)).

To explore whether $[\text{CO}_2]_{(\text{aq})}$ is an important influence on $\text{CO}_2(\varepsilon_p\text{-alk})$, I calculate predicted $[\text{CO}_2]_{(\text{aq})}$ ($[\text{CO}_2]_{(\text{aq})\text{-predicted}}$)
for each of the samples. To calculate $[\text{CO}_2]_{(\text{aq})\text{-predicted}}$, the ice core value of atmospheric CO_2 at the equivalent time interval
is used in combination with Eq. 8 to calculate $[\text{CO}_2]_{(\text{aq})}$ at the time of alkenone production. Reconstructed estimates of SST
and salinity are used as for $\text{CO}_2(\varepsilon_p\text{-alk})$ above, along with any estimated surface water-atmosphere disequilibrium. Points in
130 Figure 4 are then coloured by $[\text{CO}_2]_{(\text{aq})\text{-predicted}}$.

Inspection of Figure 4 suggests a connection between ($[\text{CO}_2]_{(\text{aq})\text{-predicted}}$) and the skill of $\text{CO}_2(\varepsilon_p\text{-alk})$ to reconstruct
atmospheric CO_2 , with the points clustering around the 1:1 line lighter in colour (so with higher $[\text{CO}_2]_{(\text{aq})\text{-predicted}}$), whilst
points falling away from the 1:1 line have lower $[\text{CO}_2]_{(\text{aq})\text{-predicted}}$.

To explore this relationship, I progressively restricted the included samples on the basis of $[\text{CO}_2]_{(\text{aq})\text{-predicted}}$, and at each
135 stage calculated a Pearson correlation co-efficient for each subset. Under this analysis the correlation co-efficient progressively
increased as more of the low $[\text{CO}_2]_{(\text{aq})\text{-predicted}}$ samples were excluded (Figure 5). All analyses were performed in R (R Core
Team, 2020) using RStudio (RStudio Team, 2020).

This suggests that the fidelity of the $\text{CO}_2(\varepsilon_p\text{-alk})$ depends on the concentration of $[\text{CO}_2]_{(\text{aq})}$, improving at higher levels of
 $[\text{CO}_2]_{(\text{aq})}$.

140 To further investigate this potential relationship, I progressively exclude samples based on $[\text{CO}_2]_{(\text{aq})\text{-predicted}}$ with a step
size of $0.05 \mu\text{molL}^{-1}$, again calculating Pearson correlation coefficients between ice core and $\text{CO}_2(\varepsilon_p\text{-alk})$ for each subsample
of the population. The result is shown in Figure 6. Here the analysis shows, similar to Figure 5, that as the samples with lowest
 $[\text{CO}_2]_{(\text{aq})\text{-predicted}}$ are progressively removed, the correlation between ice core and $\text{CO}_2(\varepsilon_p\text{-alk})$ increases. Furthermore, this

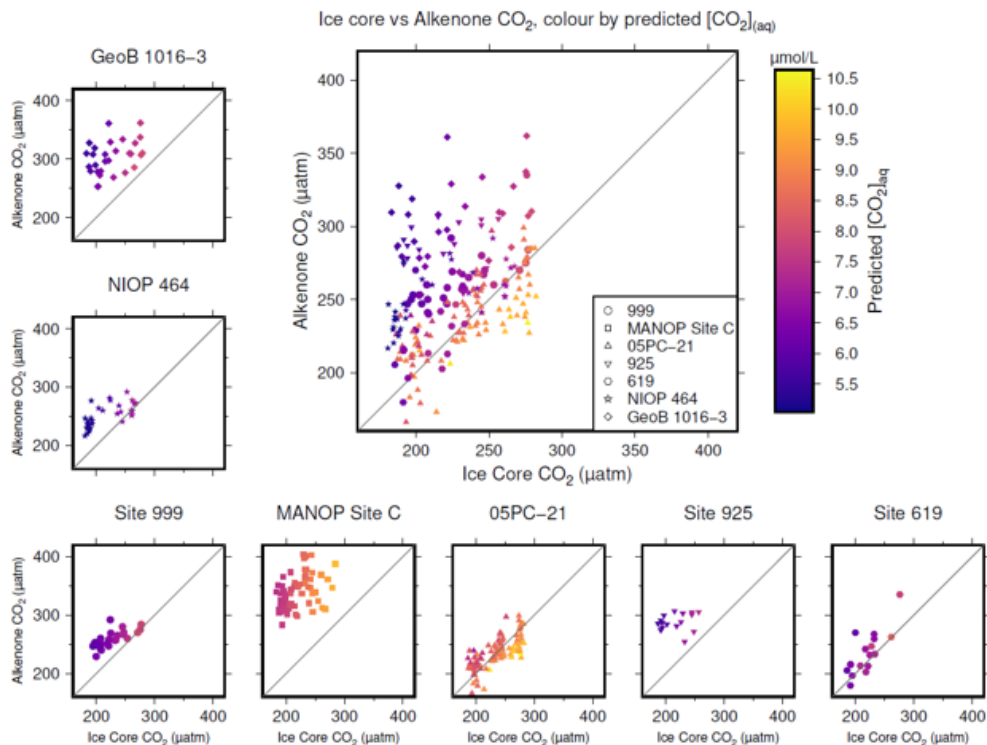


Figure 4. Crossplots of $\text{CO}_2(\epsilon_p\text{-alk})$ -based atmospheric CO_2 (y-axes vs the time-equivalent estimate from ice core records (x-axes; Bereiter et al. (2015); Table 2)). The large panel compiles all sites, with the exception of MANOP Site C, as explained in the text. Symbols are coloured by predicted $[\text{CO}_2]_{\text{aq}}$ for each site and time as explained in the text. Full sources for alkenone data are shown in Table 1. A 1:1 line is included in all plots for comparison.

continues only up until $[\text{CO}_2]_{\text{aq-predicted}}$ reaches $7 \mu\text{molL}^{-1}$. Above this, the correlation coefficient plateaus, until the subsample reaches such a small size that spurious correlations become important (Figure 6b).

3.2 Sensitivity and Uncertainty Tests

As it is not impossible that that a similar pattern could emerge if the dataset were particularly shaped so that there was increased density surrounding the 1:1 correlation line, I ran a series of sensitivity experiments. In these, rather than reducing the sample by filtering by $[\text{CO}_2]_{\text{aq-predicted}}$, the whole dataset (Table 1) was randomly ordered, and then stepwise subsampled so that the number of samples equalled the number of values for each value of $[\text{CO}_2]_{\text{aq-predicted}}$ (ie for each point in Figure 6, an equivalently sized but randomly selected sample was made such that for any equivalent value of $[\text{CO}_2]_{\text{aq-predicted}}$ the randomly ordered sample had an equivalent n as shown in Figure 6b). Pearson correlation coefficients were calculated for each subsample as above. To allow for possible age model uncertainties, a 3000 year (1σ) uncertainty was also applied to each sample. This uncertainty was applied to the age of each sample prior to sampling of the ice core record, and is

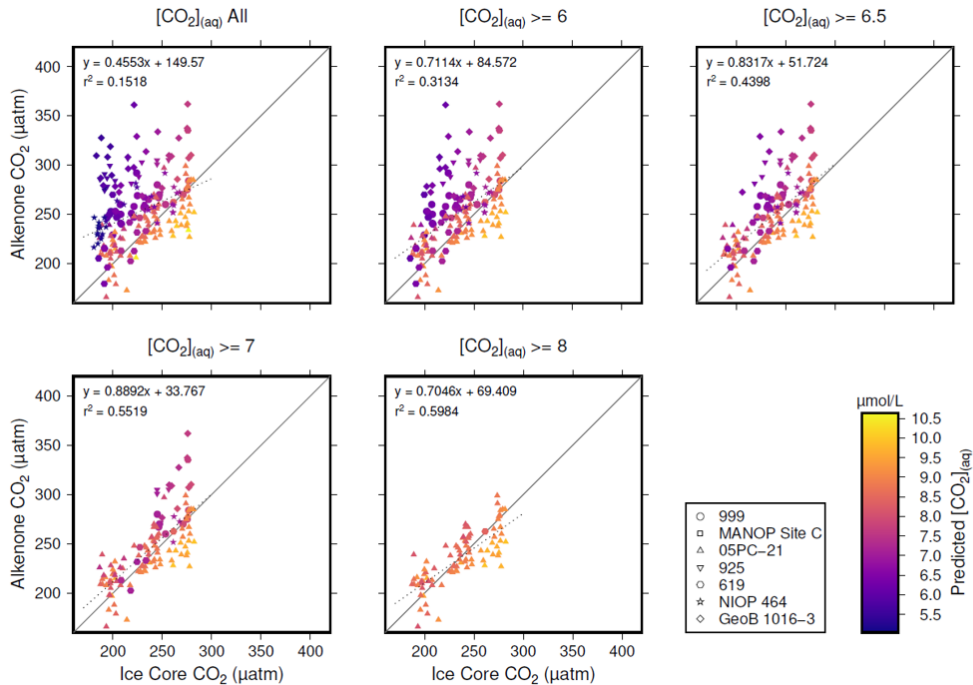


Figure 5. Crossplots of $\text{CO}_2(\varepsilon_p - \text{alk})$ -based atmospheric CO_2 (Table 1; y-axes) vs the time-equivalent estimate from ice core records (x-axes; Bereiter et al. (2015); Table 2)). The sample of published values of $\text{CO}_2(\varepsilon_p - \text{alk})$ was progressively restricted by $[\text{CO}_2]_{(\text{aq}) - \text{predicted}}$, indicated by the subplot titles. Individual values are coloured by $[\text{CO}_2]_{(\text{aq}) - \text{predicted}}$, and Sites indicated by shape (see key). Pearson correlation coefficients and equations of best fit are shown in each panel, along with a 1:1 line.

155 applied as a normally distributed uncertainty. Uncertainty in $\text{CO}_2(\varepsilon_p - \text{alk})$ measurements is typically calculated using Monte Carlo modelling of all the parameters (i.e Pagani et al. (1999); Badger et al. (2013a, b)), however this was not done in all the published work (Table 1), and some differences in approach was found across the published work. Therefore to create $\text{CO}_2(\varepsilon_p - \text{alk})$ uncertainty estimates for each value in this study, I emulate the uncertainties based on the $\text{CO}_2(\varepsilon_p - \text{alk})$ value. I built a simple emulator (Figure 7) by running Monte Carlo uncertainty estimates for all of the included datasets (Table 1) using the same estimates of uncertainty for each variable in the $\text{CO}_2(\varepsilon_p - \text{alk})$ calculation as applied in Badger et al. (2013a, b).
 160 This then allows the uncertainty to be included in the $[\text{CO}_2]_{(\text{aq}) - \text{predicted}}$ calculation as well as $\text{CO}_2(\varepsilon_p - \text{alk})$, and allowed for uncertainty estimates to be site-ambivalent.

The result is shown in Figure 8, and suggests that the $7 \mu\text{molL}^{-1}$ break point remains valid. The absolute value of r^2 is reduced, even at higher $[\text{CO}_2]_{(\text{aq}) - \text{predicted}}$, but this would be expected given the addition of uncertainty in age model, as the published age is most likely to align with the ice core. Given the rapid rate of change at deglaciations, this effect is likely to be particularly pronounced in this dataset as many records have high temporal resolution around deglaciations in order to attempt to resolve them. Any small age model offset introduced by the error modelling in these intervals also clearly has the potential
 165

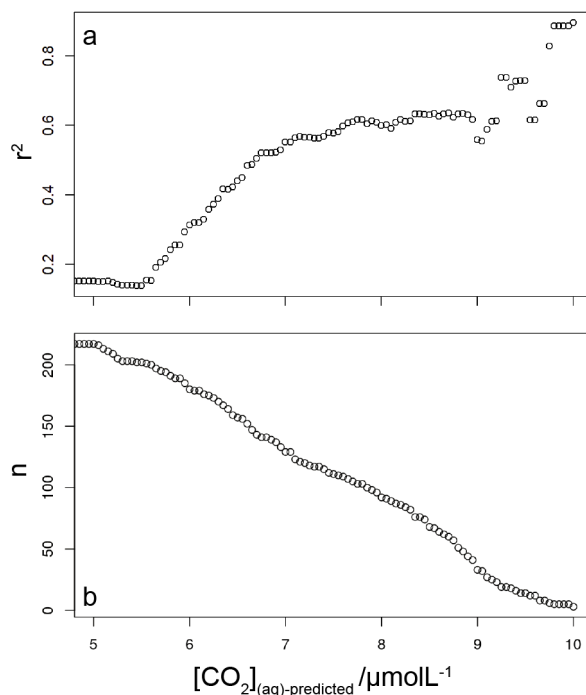


Figure 6. Pearson correlation coefficient (panel a) of a reducing sample of all compiled $\text{CO}_{2(\varepsilon_p-\text{alk})}$ (Table 1) vs the time-equivalent estimate from ice core records (Bereiter et al. (2015); Table 2). The sample reduces stepwise by $0.05 \mu\text{molL}^{-1}$, and the number of records in each subsample is shown in panel b.

to induce large differences between the $\text{CO}_{2(\varepsilon_p-\text{alk})}$ and ice core values. Figure 8 clearly demonstrates that it is the filtering by $[\text{CO}_2]_{(\text{aq})-\text{predicted}}$ rather than any spurious correlations which determine the shape of the data in Figures 6 and 8.

170 4 Discussion

The plateau in r^2 in Figures 6a and 8a suggest that below a $[\text{CO}_2]_{(\text{aq})-\text{predicted}}$ of $\sim 7 \mu\text{molL}^{-1}$ $\text{CO}_{2(\varepsilon_p-\text{alk})}$ is no longer as good a predictor of ice core CO_2 as when $[\text{CO}_2]_{(\text{aq})-\text{predicted}} > 7 \mu\text{molL}^{-1}$. This is clear from comparing the relationship between samples where $[\text{CO}_2]_{(\text{aq})-\text{predicted}} < 7 \mu\text{molL}^{-1}$ with those where $[\text{CO}_2]_{(\text{aq})-\text{predicted}} > 7 \mu\text{molL}^{-1}$ in Figure 9. Here the r^2 for the former of 0.15 is substantially less than the latter of 0.55. I suggest that this is because below this threshold, the
 175 fundamental assumption of $\text{CO}_{2(\varepsilon_p-\text{alk})}$; that carbon is passively taken up by haptophytes, no longer holds true. One obvious explanation for why this would be the case is that at low levels of $[\text{CO}_2]_{(\text{aq})}$ haptophytes have to actively uptake carbon in order to satisfy metabolic demand.

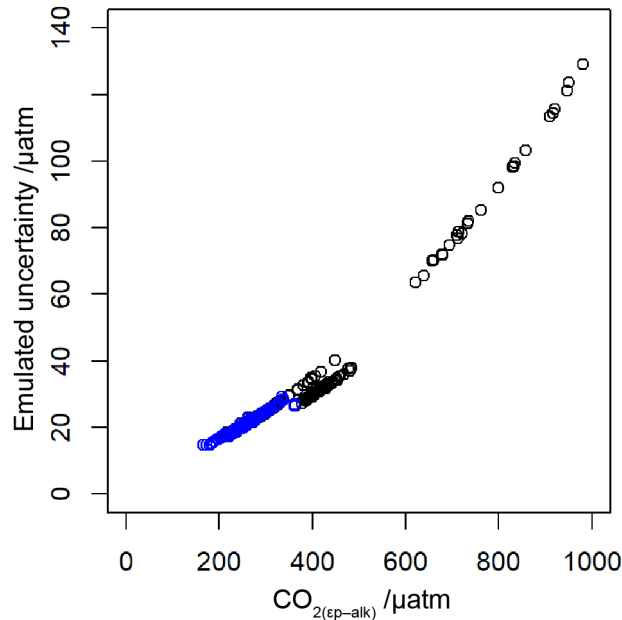


Figure 7. Emulated uncertainty in $\text{CO}_2(\varepsilon_{\text{p-alk}})$, generated by running Monte Carlo uncertainty models for all sites in Table 1 applying the same approach to uncertainty as Badger et al. (2013a, b). Estimates used in this study are highlighted in blue.

Similar behaviour has been recognised in some culture studies (Laws et al., 1997, 2002; Cassar et al., 2006), with some evidence that the diatom *Phaeodactylum tricornutum* even has a similar CCM threshold (Laws et al., 1997) but this study is the clearest evidence of the behaviour in alkenone based studies of the environment.

By applying a threshold value for $[\text{CO}_2]_{(\text{aq})-\text{predicted}}$ of $7 \mu\text{molL}^{-1}$ to the published records (Table 1) values of $\text{CO}_2(\varepsilon_{\text{p-alk}})$ which are influence by active CCMs can be eliminated. Recognition of this new threshold value of $[\text{CO}_2]_{(\text{aq})-\text{predicted}}$ allows for a new record of Pleistocene $\text{CO}_2(\varepsilon_{\text{p-alk}})$ to be compiled. This compilation then much better replicates the glacial-interglacial pattern of CO_2 change over the last 260 Ka (Figure 10). Whilst this present compilation does rely on ice core CO_2 records to estimate $[\text{CO}_2]_{(\text{aq})-\text{predicted}}$, and therefore has little direct utility as a CO_2 record, it does demonstrate that recognition of the CCM threshold allows accurate CO_2 reconstruction using $\text{CO}_2(\varepsilon_{\text{p-alk}})$. This, and the behaviour shown in Figures 6a and 8a suggests the CCMs may effectively be considered either active or not, and that when $[\text{CO}_2]_{(\text{aq})}$ is plentiful passive uptake dominates, at least sufficiently in most oceanographic settings that $\text{CO}_2(\varepsilon_{\text{p-alk}})$ can accurately record atmospheric CO_2 . This implies that if areas of the ocean (or intervals of time) with low $[\text{CO}_2]_{(\text{aq})}$ can be avoided, accurate reconstructions of atmospheric CO_2 can be acquired using $\text{CO}_2(\varepsilon_{\text{p-alk}})$.

As $[\text{CO}_2]_{(\text{aq})}$ is effected by both SST and atmospheric CO_2 , for $\text{CO}_2(\varepsilon_{\text{p-alk}})$ to be effective in reconstructing atmospheric CO_2 , areas of warm water (i.e. tropical or shallow shelf regions) under relatively low atmospheric CO_2 must be avoided. However, as the atmospheric CO_2 control renders the global surface ocean sufficiently replete in $[\text{CO}_2]_{(\text{aq})}$ at Pliocene-like levels

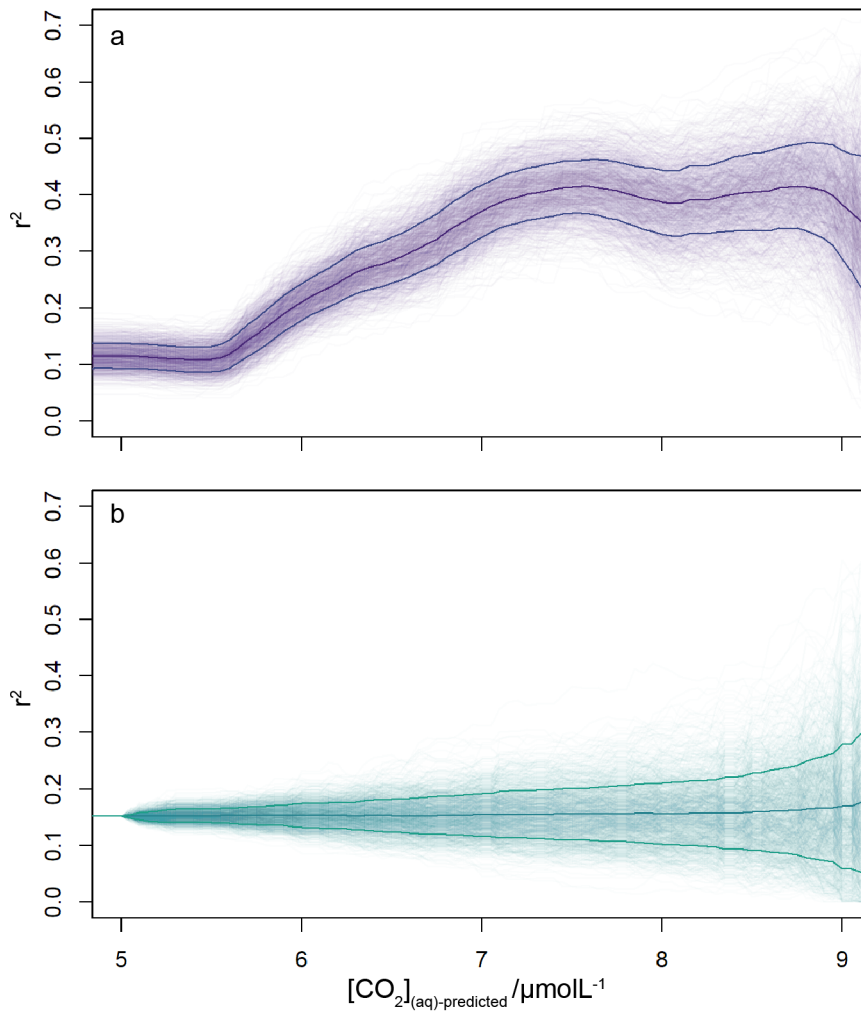


Figure 8. Pearson correlation coefficient of a reducing sample of all compiled $\text{CO}_{2(\varepsilon_p-\text{alk})}$ (Table 1) vs the time-equivalent estimate from ice core records (Bereiter et al. (2015); Table 2). As in Figure 6 the sample reduces stepwise by $0.05 \mu\text{molL}^{-1}$. Panel a shows a 1000 member Monte Carlo analysis, whereby uncertainty in $\text{CO}_{2(\varepsilon_p-\text{alk})}$ and age is considered, as detailed in the text. Panel b shows a similar 1000 member Monte Carlo analysis, but with random sampling of the whole $\text{CO}_{2(\varepsilon_p-\text{alk})}$ population so that the number of samples is equivalent to the dataset shown in panel a, ie the size of the sample follows that shown in Figure 6b. Means and one σ uncertainties are shown as the bold lines.

of atmospheric CO_2 and above (Martínez-Botí et al., 2015) at all but the warmest surface ocean temperatures, $\text{CO}_{2(\varepsilon_p-\text{alk})}$ is likely to be a reliable system for most of the Cenozoic. It is only in the Pleistocene that atmospheric CO_2 is low enough for CCMs to be widely active across the surface ocean, with the low CO_2 glacials providing the most difficulty (Badger et al., 2019). This finding aligns well with evidence that CCMs developed in coccolithophores as a response to declining atmospheric

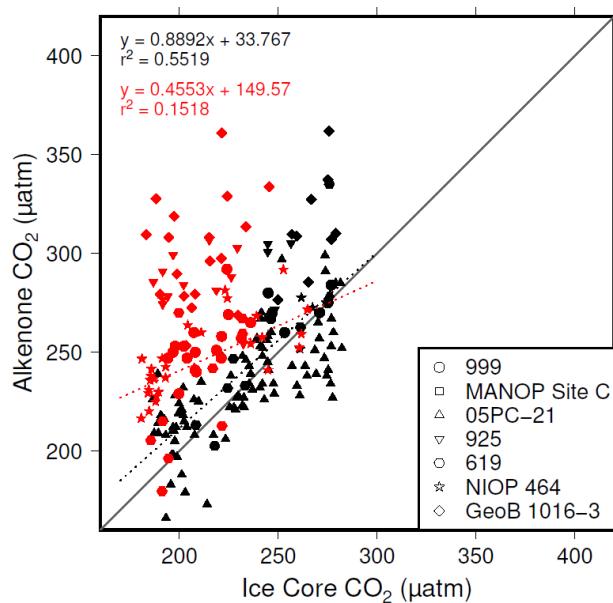


Figure 9. Correlations between $\text{CO}_2(\varepsilon_{\text{p-alk}})$ and ice core CO_2 where $[\text{CO}_2]_{(\text{aq})-\text{predicted}} > 7 \mu\text{molL}^{-1}$ (black symbols) and $[\text{CO}_2]_{(\text{aq})-\text{predicted}} < 7 \mu\text{molL}^{-1}$ (red symbols).

CO_2 through the Cenozoic, and were developing in $[\text{CO}_2]_{(\text{aq})}$ -limited parts of the ocean in the late Miocene at the earliest, and likely not widespread until the Plio-Pleistocene (Bolton et al., 2012; Bolton and Stoll, 2013).

200 Recent has attempted to correct for the existence of CCMs in palaeo-records of atmospheric CO_2 (Zhang et al., 2019; Stoll et al., 2019; Zhang et al., 2020). However, these assume that CCMs are always active, and that Pleistocene records can be used to correct for them throughout the Cenozoic. If, as suggested by the analyses presented here, CCMs *only* act at low $[\text{CO}_2]_{(\text{aq})}$, and largely only in conditions prevalent through the late Pliocene and Pleistocene, it is plausible that corrections based on
 205 uptake inherent in $\text{CO}_2(\varepsilon_{\text{p-alk}})$ as traditionally applied may still be valid.

5 Conclusions

Reconstructions of past atmospheric CO_2 with proxy tools like $\text{CO}_2(\varepsilon_{\text{p-alk}})$ are critical to understanding how the Earth's climate system operates, so long as the tools used can be relied upon to be accurate and precise. This re-analysis of existing Pleistocene $\text{CO}_2(\varepsilon_{\text{p-alk}})$ records reveals that below a critical threshold of $[\text{CO}_2]_{(\text{aq})}$ of $7 \mu\text{molL}^{-1}$ the relationship between
 210 $\delta^{13}\text{C}_{\text{alkenone}}$ and atmospheric CO_2 breaks down, plausibly because below this threshold haptophytes are able to actively update carbon using CCMs in order to satisfy metabolic demand.

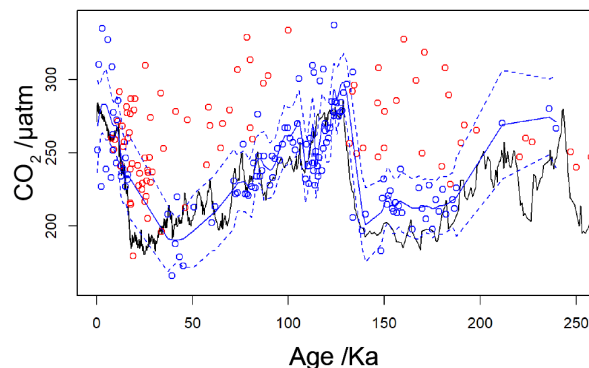


Figure 10. Revised compilation of Pleistocene $\text{CO}_2(\varepsilon_{\text{p-alk}})$ vs ice core records. The compiled published records (Table 1) are shown as circles, coloured red where $[\text{CO}_2]_{(\text{aq})-\text{predicted}}$ is below a threshold of $7 \mu\text{mol L}^{-1}$, and blue where $[\text{CO}_2]_{(\text{aq})-\text{predicted}} > 7 \mu\text{mol L}^{-1}$. The solid blue line is a loess filter (span 0.1) through the $[\text{CO}_2]_{(\text{aq})-\text{predicted}} > 7 \mu\text{mol L}^{-1}$ values, with 95 % confidence intervals (dashed blue line). The black line is the ice core compilation of Bereiter et al. (2015) (Table 2).

Although reconstructing the low levels of atmospheric CO_2 in the Pleistocene glacials and areas of the global ocean where $[\text{CO}_2]_{(\text{aq})}$ is less than $7 \mu\text{mol L}^{-1}$ will be impossible, for much of the Cenozoic the $\text{CO}_2(\varepsilon_{\text{p-alk}})$ proxy retains utility. If care is taken to avoid regions and oceanographic settings where $[\text{CO}_2]_{(\text{aq})}$ may be expected abnormally low, $\text{CO}_2(\varepsilon_{\text{p-alk}})$ remains an
 215 important and useful proxy to understand the Earth system.

Author contributions. MPSB conceived the study, designed the methodology, analysed the data, prepared the figures and wrote the manuscript (conceptualization, formal analysis, investigation, methodology, visualization, writing - original draft, review and editing)

Competing interests. MPSB declares that he has no conflict of interest

Acknowledgements. I am grateful to Gavin Foster and Tom Chalk for frequent and stimulating discussions on alkenone paleobarometry. I
 220 thank all authors who made full datasets available online. I thank Kirsty Edgar for comments on various drafts that greatly improved this manuscript.

References

- Ahn, J. and Brook, E. J.: Siple Dome ice reveals two modes of millennial CO₂ change during the last ice age, *Nature Communications*, 5, 3723, <http://dx.doi.org/10.1038/ncomms4723>, 2014.
- 225 Anagnostou, E., John, E. H., Edgar, K. M., Foster, G. L., Ridgwell, A., Inglis, G. N., Pancost, R. D., Lunt, D. J., and Pearson, P. N.: Changing atmospheric CO₂ concentration was the primary driver of early Cenozoic climate, *Nature*, 533, 380–384, <https://doi.org/10.1038/nature17423>, <http://www.nature.com/doi/10.1038/nature17423>, 2016.
- Andersen, N., Miiller, P. J., Kirsf, G., and Schneider, R. R.: Alkenone delta-13C as a proxy for past pCO₂ in surface waters: Results from the Late Quaternary Angola Current, 1999.
- 230 Antonov, J. I., Seidov, D., Boyer, T. P., Locarnini, R. A., Mishonov, A. V., Garcia, H. E., Baranova, O. K., Zweng, M. M., and Johnson, D. R.: World Ocean Atlas 2009, Volume 2: Salinity, <https://doi.org/10.1182/blood-2011-06-357442>, 2010.
- Badger, M. P., Lear, C. H., Pancost, R. D., Foster, G. L., Bailey, T. R., Leng, M. J., and Abels, H. a.: CO₂ drawdown following the middle Miocene expansion of the Antarctic Ice Sheet, *Paleoceanography*, 28, 42–53, <https://doi.org/10.1002/palo.20015>, 2013a.
- Badger, M. P., Foster, G. L., Chalk, T. B., Gibbs, S. J., Badger, M. P. S., Pancost, R. D., Schmidt, D. N., Sexton, P. F., Mackensen, A., Bown, P. R., and Pälike, H.: Insensitivity of alkenone carbon isotopes to atmospheric CO₂ at low to moderate CO₂ levels, *Climate of the Past*, 15, 539–554, <https://doi.org/10.5194/cp-2018-152>, 2019.
- Badger, M. P. S., Schmidt, D. N., Mackensen, A., and Pancost, R. D.: High-resolution alkenone palaeobarometry indicates relatively stable pCO₂ during the Pliocene (3.3–2.8 Ma), *Philosophical transactions. Series A, Mathematical, physical, and engineering sciences*, 371, 20130094, <https://doi.org/10.1098/rsta.2013.0094>, <http://www.ncbi.nlm.nih.gov/pubmed/24043868>, 2013b.
- 240 Bae, S. W., Lee, K. E., and Kim, K.: Use of carbon isotopic composition of alkenone as a CO₂ proxy in the East Sea/Japan Sea, *Continental Shelf Research*, 107, 24–32, <https://doi.org/10.1016/j.csr.2015.07.010>, <https://www.sciencedirect.com/science/article/pii/S0278434315300133?via%3Dihubhttps://linkinghub.elsevier.com/retrieve/pii/S0278434315300133>, 2015.
- Beerling, D. J. and Royer, D. L.: Convergent Cenozoic CO₂ history, *Nature Geoscience*, 4, 418–420, <https://doi.org/10.1038/ngeo1186>, <http://dx.doi.org/10.1038/ngeo1186>, 2011.
- 245 Bereiter, B., Lüthi, D., Siegrist, M., Schüpbach, S., Stocker, T. F., and Fischer, H.: Mode change of millennial CO₂ variability during the last glacial cycle associated with a bipolar marine carbon seesaw, *Proceedings of the National Academy of Sciences*, 109, 9755–9760, <https://doi.org/10.1073/pnas.1204069109>, <http://www.pnas.org/content/109/25/9755.abstract>, 2012.
- Bereiter, B., Eggleston, S., Schmitt, J., Nehrbass-Ahles, C., Stocker, T. F., Fischer, H., Kipfstuhl, S., and Chappellaz, J.: Revision of the EPICA Dome C CO₂ record from 800 to 600 kyr before present, *Geophysical Research Letters*, 42, 542–549, <https://doi.org/10.1002/2014GL061957>, <http://doi.wiley.com/10.1002/2014GL061957>, 2015.
- 250 Bidigare, R., Fluegge, A., Freeman, K. H., Hanson, K., Hayes, J. M., Hollander, D., Jasper, J. P., King, L. L., Laws, E., Milder, J., Millero, F. J., Pancost, R., Popp, B. N., Steinberg, P., and Wakeham, S. G.: Consistent fractionation of ¹³C in nature and in the laboratory: Growth-rate effects in some haptophyte algae, *Global Biogeochemical Cycles*, 11, 279–292, <http://onlinelibrary.wiley.com/doi/10.1029/96GB03939/full>, 1997.
- 255 Bolton, C. T. and Stoll, H. M.: Late Miocene threshold response of marine algae to carbon dioxide limitation., *Nature*, 500, 558–62, <https://doi.org/10.1038/nature12448>, <http://www.ncbi.nlm.nih.gov/pubmed/23985873>, 2013.

- Bolton, C. T., Stoll, H. M., and Mendez-Vicente, A.: Vital effects in coccolith calcite: Cenozoic climate- p CO₂ drove the diversity of carbon acquisition strategies in coccolithophores?, *Paleoceanography*, 27, n/a–n/a, <https://doi.org/10.1029/2012PA002339>, <http://doi.wiley.com/10.1029/2012PA002339>, 2012.
- 260 Brassell, S., Eglinton, G., and Marlowe, I.: Molecular stratigraphy: a new tool for climatic assessment, *Nature*, 320, 129–133, http://www.geology.fsu.edu/~odom/orbitalforcingstratigraphy/Brassell-Original_{_}Alkenone_{_}Paper-Na86.pdf, 1986.
- Cassar, N., Laws, E. a., and Popp, B. N.: Carbon isotopic fractionation by the marine diatom *Phaeodactylum tricornutum* under nutrient- and light-limited growth conditions, *Geochimica et Cosmochimica Acta*, 70, 5323–5335, <https://doi.org/10.1016/j.gca.2006.08.024>, <http://linkinghub.elsevier.com/retrieve/pii/S0016703706020084>, 2006.
- 265 Conte, M. H., Volkman, J. K., and Eglinton, G.: Lipid biomarkers of the Haptophyta, in: *The Haptophyte algae*, edited by Green, J. and Leadbeater, B., pp. 351–377, Oxford University Press, UK, 1994.
- Farrimond, P., Eglinton, G., and Brassell, S. C.: Alkenones in Cretaceous black shales, Blake-Bahama Basin, western North Atlantic, *Organic Geochemistry*, 10, 897–903, [https://doi.org/10.1016/S0146-6380\(86\)80027-4](https://doi.org/10.1016/S0146-6380(86)80027-4), 1986.
- Foster, G. L., Lear, C. H., and Rae, J. W. B.: The evolution of pCO₂, ice volume and climate during the middle Miocene, *Earth and Planetary Science Letters*, 341–344, 243–254, <https://doi.org/10.1016/j.epsl.2012.06.007>, <http://linkinghub.elsevier.com/retrieve/pii/S0012821X12002919>, 2012.
- 270 Foster, G. L., Royer, D. L., and Lunt, D. J.: Future climate forcing potentially without precedent in the last 420 million years, *Nature Communications*, 8, 14 845, <https://doi.org/10.1038/ncomms14845>, <http://www.nature.com/doi/10.1038/ncomms14845>, 2017.
- Garcia, H. E., Locarnini, R. A., Boyer, T. P., Antonov, J. I., Baranova, O. K., Zweng, M. M., Reagan, J. R., and Johnson, D. R.: *World Ocean Atlas 2013, Volume 4 : Dissolved Inorganic Nutrients (phosphate, nitrate, silicate)*, 2013.
- 275 Gradstein, F., Ogg, J., Schmitz, M., and Ogg, G.: *The Geologic Time Scale 2012*, Elsevier, 1 edn., 2012.
- Jasper, J. and Hayes, J.: A carbon isotope record of CO₂ levels during the late Quaternary, *Nature*, 347, 462–464, <http://www.nature.com/nature/journal/v347/n6292/abs/347462a0.html>, 1990.
- Jasper, J., Hayes, J., Mix, A., and Prahl, F.: Photosynthetic fractionation of ¹³C and concentrations of dissolved CO₂ in the central equatorial Pacific during the last 255,000 years, *Paleoceanography*, 9, 781–798, <http://onlinelibrary.wiley.com/doi/10.1029/94PA02116/full>, 1994.
- 280 Kürschner, W. M., Kvacek, Z., and Dilcher, D. L.: The impact of Miocene atmospheric carbon dioxide fluctuations on climate and the evolution, *Proceedings of the National Academy of Sciences of the United States of America*, 105, 449–453, 2008.
- Laws, E., Popp, B., Bidigare, R., Kennicutt, M., and Macko, S.: Dependence of phytoplankton carbon isotopic composition on growth rate and [CO₂]_{aq}: Theoretical considerations and experimental, *Geochimica et Cosmochimica Acta*, 59, 1131–1138, <http://www.sciencedirect.com/science/article/pii/S0016703795000304>, 1995.
- 285 Laws, E. a., Bidigare, R. R., and Popp, B. N.: Effect of growth rate and CO₂ concentration on carbon isotopic fractionation by the marine diatom *Phaeodactylum tricornutum*, *Limnology and Oceanography*, 42, 1552–1560, <https://doi.org/10.4319/lo.1997.42.7.1552>, <http://doi.wiley.com/10.4319/lo.1997.42.7.1552>, 1997.
- Laws, E. a., Popp, B. N., Cassar, N., and Tanimoto, J.: ¹³C discrimination patterns in oceanic phytoplankton: likely influence of CO₂ concentrating mechanisms, and implications for palaeoreconstructions, *Functional Plant Biology*, 29, 323–333, <https://doi.org/10.1071/Pp01183>, 2002.
- 290 Locarnini, R. A., Mishonov, A. V., Antonov, J. I., Boyer, T. P., Garcia, H. E., Baranova, O. K., Zweng, M. M., Paver, C. R., Reagan, J. R., Johnson, D. R., Hamilton, M., and Seidov, D.: *World Ocean Atlas 2013. Vol. 1: Temperature.*, Tech. rep., <https://doi.org/10.1182/blood-2011-06-357442>, 2013.

- 295 MacFarling Meure, C., Etheridge, D., Trudinger, C., Steele, P., Langenfelds, R., van Ommen, T., Smith, A., and Elkins, J.:
Law Dome CO₂, CH₄ and N₂O ice core records extended to 2000 years BP, *Geophysical Research Letters*, 33, L14810,
<https://doi.org/10.1029/2006gl026152>, <http://dx.doi.org/10.1029/2006GL026152>, 2006.
- Marcott, S. A., Bauska, T. K., Buizert, C., Steig, E. J., Rosen, J. L., Cuffey, K. M., Fudge, T. J., Severinghaus, J. P., Ahn, J., Kalk, M. L.,
McConnell, J. R., Sowers, T., Taylor, K. C., White, J. W. C., and Brook, E. J.: Centennial-scale changes in the global carbon cycle during
300 the last deglaciation, *Nature*, 514, 616–619, <http://dx.doi.org/10.1038/nature13799>, 2014.
- Marlowe, I., Brassell, S., Eglinton, G., and Green, J.: Long-chain alkenones and alkyl alkenoates and the fossil coccolith record of marine
sediments, *Chemical Geology*, 88, 349–375, [https://doi.org/10.1016/0009-2541\(90\)90098-R](https://doi.org/10.1016/0009-2541(90)90098-R), <http://linkinghub.elsevier.com/retrieve/pii/000925419090098R>, 1990.
- Martínez-Botí, M. A., Foster, G. L., Chalk, T. B., Rohling, E. J., Sexton, P. F., Lunt, D. J., Pancost, R. D., Badger, M. P.,
305 and Schmidt, D. N.: Plio-Pleistocene climate sensitivity evaluated using high-resolution CO₂ records, *Nature*, 518, 49–54,
<https://doi.org/10.1038/nature14145>, <http://dx.doi.org/10.1038/nature14145>, 2015.
- Monnin, E., Indermuhle, A., Dallenbach, A., Fluckiger, J., Stauffer, B., Stocker, T. F., Raynaud, D., and Barnola, J. M.: Atmospheric CO₂
concentrations over the last glacial termination, *Science*, 291, 112–114, <https://doi.org/10.1126/science.291.5501.112>, 2001.
- Monnin, E., Steig, E. J., Siegenthaler, U., Kawamura, K., Schwander, J., Stauffer, B., Stocker, T. F., Morse, D. L., Barnola, J.-M.,
310 Bellier, B., Raynaud, D., and Fischer, H.: Evidence for substantial accumulation rate variability in Antarctica during the Holocene,
through synchronization of CO₂ in the Taylor Dome, Dome C and DML ice cores, *Earth and Planetary Science Letters*, 224, 45–54,
<https://doi.org/10.1016/j.epsl.2004.05.007>, <http://linkinghub.elsevier.com/retrieve/pii/S0012821X04003115>, 2004.
- Mook, W. G., Bommerson, J. C., and Staverman, W. H.: Carbon isotope fractionation between dissolved bicarbonate and gaseous carbon
dioxide, *Earth and Planetary Science Letters*, 22, 169–176, [https://doi.org/10.1016/0012-821X\(74\)90078-8](https://doi.org/10.1016/0012-821X(74)90078-8), 1974.
- 315 Pagani, M., Freeman, K., and Arthur, M.: Late Miocene atmospheric CO₂ concentrations and the expansion of C₄ grasses, *Science*, 285,
876–879, <http://www.sciencemag.org/content/285/5429/876.short>, 1999.
- Pagani, M., Zachos, J. C., Freeman, K. H., Tipple, B., and Bohaty, S.: Marked decline in atmospheric carbon dioxide concentrations during
the Paleogene., *Science (New York, N.Y.)*, 309, 600–603, <https://doi.org/10.1126/science.1110063>, <http://www.ncbi.nlm.nih.gov/pubmed/15961630>, 2005.
- 320 Pagani, M., Liu, Z., LaRiviere, J., and Ravelo, A. C.: High Earth-system climate sensitivity determined from Pliocene carbon dioxide
concentrations, *Nature Geoscience*, 3, 27–30, <https://doi.org/10.1038/ngeo724>, <http://www.nature.com/doi/10.1038/ngeo724>, 2009.
- Pagani, M., Huber, M., Liu, Z., Bohaty, S. M., Henderiks, J., Sijp, W., Krishnan, S., and DeConto, R. M.: The role of carbon dioxide during
the onset of Antarctic glaciation., *Science (New York, N.Y.)*, 334, 1261–4, <https://doi.org/10.1126/science.1203909>, <http://www.ncbi.nlm.nih.gov/pubmed/22144622>, 2011.
- 325 Palmer, M. R., Brummer, G. J., Cooper, M. J., Elderfield, H., Greaves, M. J., Reichert, G. J., Schouten, S., and Yu, J. M.: Multi-
proxy reconstruction of surface water pCO₂ in the northern Arabian Sea since 29ka, *Earth and Planetary Science Letters*, 295, 49–57,
<https://doi.org/10.1016/j.epsl.2010.03.023>, <http://linkinghub.elsevier.com/retrieve/pii/S0012821X10002049>, 2010.
- Pearson, P. N., Foster, G. L., and Wade, B. S.: Atmospheric carbon dioxide through the Eocene-Oligocene climate transition., *Nature*, 461,
1110–1113, <https://doi.org/10.1038/nature08447>, <http://www.ncbi.nlm.nih.gov/pubmed/19749741>, 2009.
- 330 Petit, J. R., Jouzel, J., Raynaud, D., Barkov, N. I., Barnola, J.-M., Basile, I., Bender, M., Chappellaz, J., Davis, M., Delaygue, G., Delmotte,
M., Kotlyakov, V. M., Legrand, M., Lipenkov, V. Y., Lorius, C., Pepin, K., Ritz, C., Saltzman, E., and Stievenard, M.: Climate and

- atmospheric history of the past 420,000 years from the Vostok ice core, Antarctica, *Nature*, 399, 429–436, <http://www.nature.com/nature/journal/v399/n6735/abs/399429a0.html>, 1999.
- 335 Popp, B., Laws, E., Bidigare, R., Dore, J., Hanson, K., and Wakeham, S. G.: Effect of phytoplankton cell geometry on carbon isotopic fractionation, *Geochimica et Cosmochimica Acta*, 62, 67–77, <http://www.sciencedirect.com/science/article/pii/S0016703797003335>, 1998.
- R Core Team: R: A language and environment for statistical computing, <https://www.r-project.org/>, 2020.
- Raffi, I., Backman, J., Fornaciari, E., Pälke, H., Rio, D., Lourens, L., and Hilgen, F.: A review of calcareous nannofossil astrobiochronology encompassing the past 25 million years☆, *Quaternary Science Reviews*, 25, 3113–3137, <https://doi.org/10.1016/j.quascirev.2006.07.007>, <http://linkinghub.elsevier.com/retrieve/pii/S0277379106002320>, 2006.
- 340 Rechka, J. and Maxwell, J.: Characterisation of alkenone temperature indicators in sediments and organisms, *Organic Geochemistry*, 13, 727–734, <http://www.sciencedirect.com/science/article/pii/0146638088900940>, 1987.
- Romanek, C. S., Grossman, E. L., and Morse, J. W.: Carbon isotopic fractionation in synthetic aragonite and calcite: Effects of temperature and precipitation rate, *Geochimica et Cosmochimica Acta*, 56, 419–430, [https://doi.org/10.1016/0016-7037\(92\)90142-6](https://doi.org/10.1016/0016-7037(92)90142-6), <http://linkinghub.elsevier.com/retrieve/pii/0016703792901426>, 1992.
- 345 RStudio Team: RStudio: Integrated Development for R, <http://www.rstudio.com/>, 2020.
- Rubino, M., Etheridge, D. M., Trudinger, C. M., Allison, C. E., Battle, M. O., Langenfelds, R. L., Steele, L. P., Curran, M., Bender, M., White, J. W. C., Jenk, T. M., Blunier, T., and Francey, R. J.: A revised 1000 year atmospheric $\delta^{13}\text{C}$ -CO₂ record from Law Dome and South Pole, Antarctica, *Journal of Geophysical Research: Atmospheres*, 118, 8482–8499, <https://doi.org/10.1002/jgrd.50668>, <http://dx.doi.org/10.1002/jgrd.50668>, 2013.
- 350 Schneider, R., Schmitt, J., Köhler, P., Joos, F., and Fischer, H.: A reconstruction of atmospheric carbon dioxide and its stable carbon isotopic composition from the penultimate glacial maximum to the last glacial inception, *Climate of the Past*, 9, 2507–2523, 2013.
- Sosdian, S. M., Greenop, R., Hain, M. P., Foster, G. L., Pearson, P. N., and Lear, C. H.: Constraining the evolution of Neogene ocean carbonate chemistry using the boron isotope pH proxy, *Earth and Planetary Science Letters*, 498, 362–376, <https://doi.org/10.1016/j.epsl.2018.06.017>, <https://www.sciencedirect.com/science/article/pii/S0012821X1830356X>, 2018.
- 355 Stoll, H. M., Guitian, J., Hernandez-Almeida, I., Mejia, L. M., Phelps, S., Polissar, P., Rosenthal, Y., Zhang, H., and Ziveri, P.: Upregulation of phytoplankton carbon concentrating mechanisms during low CO₂ glacial periods and implications for the phytoplankton pCO₂ proxy, *Quaternary Science Reviews*, 208, 1–20, <https://doi.org/10.1016/j.quascirev.2019.01.012>, <https://doi.org/10.1016/j.quascirev.2019.01.012>, 2019.
- Super, J. R., Thomas, E., Pagani, M., Huber, M., Brien, C. O., and Hull, P. M.: North Atlantic temperature and pCO₂ coupling in the early-middle Miocene, *Geology*, 46, 519–522, <https://doi.org/https://doi.org/10.1130/G40228.1>, <https://pubs.geoscienceworld.org/gsa/geology/article/46/6/519/530691/North-Atlantic-temperature-and-pCO2-coupling-in>, 2018.
- Takahashi, T., Sutherland, S. C., Wanninkhof, R., Sweeney, C., Feely, R. a., Chipman, D. W., Hales, B., Friederich, G., Chavez, F., Sabine, C., Watson, A., Bakker, D. C. E., Schuster, U., Metzl, N., Yoshikawa-Inoue, H., Ishii, M., Midorikawa, T., Nojiri, Y., Körtzinger, A., Steinhoff, T., Hoppema, M., Olafsson, J., Arnarson, T. S., Tilbrook, B., Johannessen, T., Olsen, A., Bellerby, R., Wong, C. S., Delille, B., Bates, N. R., and de Baar, H. J. W.: Climatological mean and decadal change in surface ocean pCO₂, and net sea–air CO₂ flux over the global oceans, *Deep Sea Research Part II: Topical Studies in Oceanography*, 56, 554–577, <https://doi.org/10.1016/j.dsr2.2008.12.009>, <http://linkinghub.elsevier.com/retrieve/pii/S0967064508004311>, 2009.
- 365 Takahashi, T., Sutherland, S. C., Chipman, D. W., Goddard, J., Newberber, T., and Sweeney, C.: Climatological Distributions of pH, pCO₂, Total CO₂, Alkalinity, and CaCO₃ Saturation in the Global Surface Ocean, in: *Climatological Distributions of pH, pCO₂, Total CO₂, Alka-*

- 370 linity, and CaCO₃ Saturation in the Global Surface Ocean. ORNL/CDIAC-160, NDP-094, Carbon Dioxide Information Analysis Center, Oak Ridge National Laboratory, U.S. Department of Energy, Oak Ridge, Tennessee, <https://doi.org/10.3334/CDIAC/OTG.NDP094>, 2014.
- Volkman, J. K.: Ecological and environmental factors affecting alkenone distributions in seawater and sediments, *Geochemistry, Geophysics, Geosystems*, 1, n/a–n/a, <https://doi.org/10.1029/2000GC000061>, <http://doi.wiley.com/10.1029/2000GC000061>, 2000.
- Weiss, R. F.: The solubility of nitrogen, oxygen and argon in water and seawater, *Deep-Sea Research and Oceanographic Abstracts*, 17, 375 721–735, [https://doi.org/10.1016/0011-7471\(70\)90037-9](https://doi.org/10.1016/0011-7471(70)90037-9), 1970.
- Weiss, R. F.: Carbon dioxide in water and seawater: the solubility of a non-ideal gas, *Marine Chemistry*, 2, 203–215, 1974.
- Zhang, Y. G., Pagani, M., Liu, Z., Bohaty, S. M., and Deconto, R.: A 40-million-year history of atmospheric CO₂, *Philosophical transactions. Series A, Mathematical, physical, and engineering sciences*, 371, 20130096, <https://doi.org/10.1098/rsta.2013.0096>, <http://www.ncbi.nlm.nih.gov/pubmed/24043869>, 2013.
- 380 Zhang, Y. G., Pearson, A., Benthien, A., Dong, L., Huybers, P., Liu, X., and Pagani, M.: Refining the alkenone-pCO₂ method I: Lessons from the Quaternary glacial cycles, *Geochimica et Cosmochimica Acta*, 260, 177–191, <https://doi.org/10.1016/j.gca.2019.06.032>, <https://doi.org/10.1016/j.gca.2019.06.032>, 2019.
- Zhang, Y. G., Henderiks, J., and Liu, X.: Refining the alkenone-pCO₂ method II: Towards resolving the physiological parameter ‘b’, *Geochimica et Cosmochimica Acta*, 281, 118–134, <https://doi.org/10.1016/j.gca.2020.05.002>, <https://doi.org/10.1016/j.gca.2020.05.002>, 385 2020.